Chinese Journal of Natural Medicines

***Nigella sativa L.* seed extract alleviates oxidative stress–induced cellular senescence and dysfunction in melanocytes**

Ben Niu, Xiaohong An, Yongmei Chen, Ting He, Xiao Zhan, Xiuqi Zhu, Fengfeng Ping, Wei Zhang, Jia Zhou

Citation: Ben Niu, Xiaohong An, Yongmei Chen, Ting He, Xiao Zhan, Xiuqi Zhu, Fengfeng Ping, Wei Zhang, Jia Zhou, *Nigella sativa* L. seed extract alleviates oxidative stress–induced cellular senescence and dysfunction in melanocytes, Chinese Journal of Natural Medicines, 2025, 23(2), 203–213. doi: 10.1016/S1875–5364(25)60824–7.

View online: https://doi.org/10.1016/S1875–5364(25)60824–7

Chinese Journal of Natural Medicines 23 (2025) 203-213

Contents lists available at ScienceDirect

Chinese Journal of Natural Medicines

journal homepage: www.cjnmcpu.com/

Original article

Nigella sativa L. seed extract alleviates oxidative stress-induced cellular senescence and dysfunction in melanocytes

Ben Niu[a,b,Δ], Xiaohong An[c,Δ], Yongmei Chen[a], Ting He[d], Xiao Zhan[a], Xiuqi Zhu[a], Fengfeng Ping[b], Wei Zhang[e,*], Jia Zhou[a,*]

[a] *School of Traditional Chinese Pharmacy, China Pharmaceutical University, Nanjing 211198, China*
[b] *Wuxi People's Hospital, Nanjing Medical University, Wuxi 214023, China*
[c] *Yunnan Characteristic Plant Extraction Laboratory, Yunnan Yunke Characteristic Plant Extraction Laboratory Co., Ltd., Kunming 650106, China*
[d] *Drug Discovery and Development Laboratories, Ningxia Hui Medicine Research Institute, Yinchuan, 750021, China*
[e] *Hospital for Skin Diseases Institute of Dermatology, Chinese Academy of Medical Sciences & Peking Union Medical College, Nanjing 210042, China*

ARTICLE INFO

Article history:
Received 26 April 2024
Revised 29 June 2024
Accepted 19 July 2024
Available online 20 February 2025

Keywords:
Nigella sativa L. seed extract (HZC)
Melanin
ROS
Vitiligo
Cellular senescence

ABSTRACT

Nigella sativa L. seeds have been traditionally utilized in Chinese folk medicine for centuries to treat vitiligo. This study revealed that the ethanolic extract of *Nigella sativa* L. (HZC) enhances melanogenesis and mitigates oxidative stress-induced cellular senescence and dysfunction in melanocytes. In accordance with established protocols, the ethanol fraction from *Nigella sativa* L. seeds was extracted, concentrated, and lyophilized to evaluate its herbal effects *via* 3-(4,5-dimethylthiazol-2-yl)-2,5-diphenyltetrazolium bromide (MTT) assays, tyrosinase activity evaluation, measurement of cellular melanin contents, scratch assays, senescence-associated β-galactosidase (SA-β-gal) staining, enzyme-linked immunosorbent assay (ELISA), and Western blot analysis for expression profiling of experimentally relevant proteins. The results indicated that HZC significantly enhanced tyrosinase activity and melanin content while notably increasing the protein expression levels of Tyr, Mitf, and gp100 in B16F10 cells. Furthermore, HZC effectively mitigated oxidative stress-induced cellular senescence, improved melanocyte condition, and rectified various functional impairments associated with melanocyte dysfunction. These findings suggest that HZC increases melanin synthesis in melanocytes through the activation of the MAPK, PKA, and Wnt signaling pathways. In addition, HZC attenuates oxidative damage induced by H_2O_2 therapy by activating the nuclear factor E2-related factor 2-antioxidant response element (Nrf2-ARE) pathway and enhancing the activity of downstream antioxidant enzymes, thus preventing premature senescence and dysfunction in melanocytes.

1. Introduction

Vitiligo is an acquired pigmentary disorder of unknown etiology, characterized by the development of white macule-like skin lesions resulting from structural and functional disruption of melanocytes [1]. Although this chronic condition does not directly threaten patients' lives, it significantly impacts their psychological well-being and quality of life, potentially increasing the risk of psychiatric disorders. Regarding the pathogenesis of vitiligo, numerous researchers have identified oxidative stress-induced melanocyte toxicity and melanocyte shedding as key factors [2]. The oxidative stress theory posits that reactive oxygen species (ROS) attack melanocytes, disrupting their normal metabolic processes, proliferation, and differentiation. This leads to premature senescence and impairment of normal physiological functions [3], including reduced melanin synthesis, decreased dendrite size, diminished adhesion, and compromised migration ability. Consequently, these factors contribute to melanocyte loss, reduced melanin content in the affected area, and the formation of characteristic white spots.

Melanocytes are dendritic cells found in various human tissues, including the skin, mucous membranes, retina, soft meninges, gallbladder, and ovaries, where melanin is produced in melanocyte melanosomes [4]. Melanin, the primary determinant of skin and hair color in humans, also protects the skin from DNA damage caused by UV radiation [5]. The process of melanogenesis is influenced by several signaling pathways, such as MAPK, cAMP/PKA, Wnt/β-catenin, PI3K/Akt, and SCF/c-Kit pathways [6]. Research has shown that vitiligo patients exhibit disrupted expression of melanogenesis-regulating factors in lesions, leading to hypopigmentation and the formation of white spots [7, 8]. In the human epidermis, a single melanocyte associates with 10–36 surrounding keratinocytes through dendrites, forming a melanin unit structure. This structure facilitates the transport of melanin from melanocytes to keratinocytes for skin coloration. Addition-

* Corresponding author.
E-mail addresses: ifmtjoel@163.com (W. Zhang); zjcpu2016@163.com (J. Zhou)
Δ These authors contributed equally to this work.

https://doi.org/10.1016/S1875-5364(25)60824-7

ally, the extension of dendrites enables melanocytes to adhere fully to the basal layer [9]. Melanocyte detachment occurs when these cells become vulnerable to mechanical stress due to weakened adhesion to keratinocytes or the basal lamina [10]. This process affects multiple intracellular signaling pathways, inducing detachment from the basal layer and eventual transepidermal loss, resulting in a reduction of melanocyte numbers and the formation of white spots. When exposed to external stimuli, the transepidermal loss of melanocytes with weakened adhesion primarily involves two aspects: loss of dendrites and defective adhesion. Kumar et al. observed that melanocytes in active vitiligo lesions were predominantly in a detached state, with microscopic examination revealing large, retracted dendrites in the perinuclear region, making patients susceptible to mechanical stress-induced transepidermal loss of melanocytes [11]. Cadherins, a family of transmembrane proteins, mediate Ca^{2+}-dependent cell-cell adhesion [12], epithelial-type calreticulin (*E*-cadherin) is a primary mediator of adhesion between melanocytes and keratinocytes in the normal human epidermis. Cario et al. reported that multiple factors cause a reduction in *E*-cadherin expression in vitiligo lesions, resulting in decreased melanocyte adhesion [13].

The nuclear factor E2-related factor 2-antioxidant response element (Nrf2-ARE) pathway represents a crucial defense mechanism against oxidative stress damage in cells, playing a significant role in mitigating such damage in melanocytes [14]. Nrf2, a member of the CNC (Cap-N-Collar) transcription factor family, regulates the expression of various antioxidant factors, including GCL, HO-1, and NQO1 [15]. Under normal physiological conditions, Nrf2 remains in a relatively inhibited state, bound to the cytoplasmic chaperone protein Keap1. Upon oxidative stimulation, Nrf2 and Keap1 dissociate, with Nrf2 undergoing phosphorylation by various protein kinases. Subsequently, Nrf2 translocates to the nucleus, where it binds to nuclear-associated proteins and recognizes ARE genes. This process activates downstream antioxidant-related proteins, thereby exerting potent antioxidant effects [16].

China has a rich history of utilizing herbs for medicinal purposes, particularly in treating skin-related ailments. This tradition dates back thousands of years. *Nigella sativa* L., a species of the *Nigella* genus in the Ranunculaceae family, has been extensively used as a medicinal herb by the Uyghur people. According to *Uyghur Medicinal* records, *Nigella sativa* L. exhibits numerous beneficial properties, including the ability to induce dryness and heat, stimulate hair growth, enhance pigmentation, and demonstrate anti-inflammatory, antioxidant, immunomodulatory, anticancer, neuroprotective, antimicrobial, antihypertensive, cardioprotective, antidiabetic, gastroprotective, nephroprotective, and hepatoprotective effects. The plant's pharmacological activities are primarily attributed to its chemical constituents, which include quercetin, kaempferol, thymoquinone, thymohydroquinone, thymol, carvacrol, nigellicine, and α-hederin [17]. In the Ningxia Region of China, *Nigella sativa* L. has shown remarkable efficacy in treating vitiligo, particularly in repigmenting skin lesion areas. Sarac et al. reported improved pigmentation rates in vitiligo patients using a *Nigella sativa* L. emulsion [18]. Additionally, Ali et al. demonstrated that *Nigella sativa* L. significantly reduced skin lesion size in vitiligo patients compared with fish oil treatment [19]. However, the precise mechanism of action of *Nigella sativa* L. seeds remains unclear, though it may be related to its antioxidant properties. In this study, we found that an ethanolic extract of *Nigella sativa* L. seed (HZC) promoted melanogenesis in B16F10 cells. HZC influences melanogenesis by activating the MAPK, PKA, and Wnt pathways, and exerts an antioxidant effect *via* the Nrf2-ARE signaling pathway. This action corrects reduced melanogenesis in B16F10 cells in a model of premature senescence and detached melanocytes, improving cell status, mitigating premature senescence, and enhancing B16F10 cell migration ability, dendriticization, and cell adhesion.

2. Materials and methods

2.1. Chemicals and reagents

L-3,4-dihydroxyphenylalanine (L-DOPA) (purity ≥ 98%) and H_2O_2 (purity 3 wt.% in H_2O) were obtained from Sigma Aldrich (St. Louis, MO, USA); sodium hydroxide (NaOH) (purity ≥ 96%) was obtained from XiLONG SCIENTIFIC (Guangzhou, China), penicillin/streptomycin (P/S) was obtained from Biosharp (Hefei, China); and Dulbecco's modified Eagle medium (DMEM) and fetal bovine serum (FBS) were purchased from Gibco (Grand Island, NY, USA). Cell lysis buffer, a BCA protein assay kit, a senescence β-galactosidase staining kit (SA-β-Gal), actin-tracker green, and a mitochondrial membrane potential assay kit with JC-1 were acquired from Biyotime (Shanghai, China). A glyceraldehyde-3-phosphate dehydrogenase (GAPDH) antibody was procured from Thermo Fisher Science (Shanghai, China). Mitf, Tyr, p-p38, t-p38, p-ERK1/2, t-ERK1/2, p-JNK, t-JNK, CREB, p-CREB, and gp100 were obtained from Abcam (Cambridge, UK). Keap1, Nrf2, HO-1, NQO1, Cdc42, *E*-cadherin, p53, p21, p-GSK-3-β, t-GSK-3-β, Rac1/2/3, β-catenin, and A-β-catenin were sourced from Cell Signaling Technology (Danvers, MA, USA). The total superoxide dismutase (T-SOD) activity assay kit, malondialdehyde (MDA) colorimetric assay kit, glutathione peroxidase (GSH-Px) activity assay kit, and catalase (CAT) activity assay kit were obtained from Elabscience (Wuhan, China). All other reagents used were of the highest quality available.

2.2. Plant material

The *Nigella sativa* L. seeds were procured from the Ningxia Hui Medical Research Institute, China. The chief pharmacist, Ting He, of the Ningxia Hui Medicine Research Institute conducted the identification of the plants.

2.3. Methods

2.3.1. Preparation of the ethanolic extract of HZC

The *Nigella sativa* L. plants underwent a series of preparatory steps. They were initially sieved (60 mesh) to remove impurities, then crushed into a coarse powder and sieved again (24 mesh). A mixture of 250 g of the processed plant material and 700 mL of ethanol was prepared and left to soak overnight. The resulting leachate was collected using a percolation column, maintaining a controlled flow rate of 2–3 mL per 100 g of herb. Subsequently, the leachate was concentrated at 40 °C using a rotary evaporator to remove the solvent. The concentrated solution was then transferred to a lyophilization mixture and subjected to pre-freezing at −60 °C for 4 h. Following this, the formal lyophilization procedure was conducted. The final samples were recovered and stored at −20 °C until they were required for use in the study.

2.3.2. Cell culture and model establishment

Mouse B16F10 melanoma cells were obtained from the Chinese Academy of Sciences (CAS), China. The cells were cultured in Dulbecco's modified Eagle medium (DMEM) supplemented with 10% FBS and 1% penicillin/streptomycin, and maintained in a 37 °C incubator with 5% CO_2 [20]. Following the induction of premature senescence and detachment of B16F10 cells, they were cultured in DMEM supplemented with 2.5% FBS and exposed to H_2O_2 at a final concentration of 0.4 mmol·L^{-1} for 12 h.

2.3.3. Cell viability assay

Cell viability was assessed through the reduction of 3-(4,5-dimethylthiazol-2-yl)-2,5-diphenyltetrazolium bromide (MTT) to formazan by mitochondrial enzymes in viable cells. The procedure was as follows: after a 48-h incubation of cells in a 96-well plate, 200 μL of MTT solution (0.5 mg·mL^{-1}) was added to each well. The cells were then incubated at 37 °C in 5% CO_2 for 4 h. Subsequently, the MTT solution was removed, and 150 μL of DMSO was added to each well. The optical density (OD) was measured using a spectrophotometer (Thermo Scientific, USA) at 570 nm after pre-shaking for 5 min [21].

2.3.4. Tyrosinase activity assay

Tyrosinase activity was assessed using the L-DOPA oxidation assay as described by Smith et al. [22]. Briefly, B16F10 cells, either drug-treated or untreated, underwent lysis in a cold buffer. Following centrifugation (12 000 r·min^{-1} for 15 min), protein concentration was determined *via* the BCA method. Subsequently, 30 μg of supernatant protein was transferred to a 0.5 mL centrifuge tube, and the volume was adjusted to 100 μL using pH 6.8 PBS buffer. After vortexing, the mixture was added to a 96-well plate containing 100 μL of 0.1% L-DOPA solution. The plate was then incubated at 27 °C for 1 h in a light-protected oven. Finally, the absorbance was measured at 475 nm using a spectrophotometer (Thermo Scientific, USA).

2.3.5. Melanin content assay

The melanin content was quantified using the NaOH cleavage method [22] in B16F10 cells, both treated and untreated with the drug, after lysis in a cold buffer. Following centrifugation (12 000 r·min^{-1} for 15 min) and collection of the melanin precipitate, the melanin was solubilized in 1 mol·L^{-1} NaOH solution containing 10% DMSO at 85 °C for 20 min. The relative melanin content was subsequently determined by measuring the absorbance at 405 nm using a spectrophotometer (Thermo Scientific, USA).

2.3.6. Western blot analysis

The B16F10 cells underwent three washes in phosphate-buffered saline before lysis in cold buffer (4 °C, 20 min). The lysed cells were transferred to centrifuge tubes and subjected to centrifugation (4 °C, 12 000 r·min^{-1}, 10 min). Subsequently, the protein content of each lysate aliquot was quantified *via* the BCA method. Proteins were then separated using SDS polyacrylamide gel electrophoresis and transferred onto polyvinylidene fluoride membranes. These membranes were blocked with 5% skim milk and incubated with primary antibodies overnight at 4 °C, followed by a 1-h incubation with secondary antibodies at 25 °C. Protein visualization was achieved using an enhanced chemiluminescence detection system (Tanon4160, China). Band shadow areas were quantified using ImageJ software (National Institutes of Health, Bethesda, MD, USA). The Western blot results presented here are representative of at least three independent experiments.

2.3.7. Zebrafish assay

The zebrafish experimental protocol was approved by the animal care institution. Adult zebrafish were acquired from Shanghai Fishbio Co., Ltd. (Shanghai, China). The zebrafish were maintained in accordance with *the Zebrafish Book* [23]. Specifically, the water temperature was regulated at approximately 28.5 °C, with a daily cycle of 14 h of light and 10 h of darkness. The fish were fed twice daily, once in the morning and once in the evening. Embryos were cultured at 28.5 °C in a light incubator and were subjected to treatment with PTU (0.2 mmol·L^{-1}) or various concentrations (0.10–100 μmol·L^{-1}) of HZC from 9 to 60 hpf, or left untreated. The effects of HZC on zebrafish were observed *via* stereomicroscopy (Leica M205 FCA, Germany).

2.3.8. Cell scratch assay

Initially, cells were cultivated in a 6-well plate until they reached approximately 90% confluence. Subsequently, a 10 μL pipette tip was utilized to create three parallel lines with a perpendicular line on the plate's bottom. The cells were then removed by washing the plate three times with PBS. Observation points were selected for imaging, with the initial scratch width recorded at 0 h. Images were captured at various time points to document cell healing progress. The extent of cell healing was observed and recorded using a Nikon eclipse ts2 inverted microscope (Nikon, Japan).

2.3.9. Senescence-associated β-galactosidase (SA-β-gal) analysis and action-tracker green staining

Following treatment of B16F10 cells, senescence was evaluated using a SA-β-gal activity kit (Beyotime Institute of Biotechnology, Shanghai, China). Additionally, action-tracker green staining was conducted (excitation wavelength 496 nm, emission wavelength 516 nm). The staining results were visualized using a Nikon Eclipse TS2 inverted microscope (Nikon, Japan) and a fluorescence microscope (Evident, USA).

2.3.10. ROS levels in cells and zebrafish

The cells in the 24-well plates were incubated with DMEM containing 10% FBS for 24 h. Subsequently, different concentrations of HZC (1, 10, 20 μg·mL^{-1}) were added, and the medium was replaced with DMEM containing 2.5% FBS for 48 h. After removing the medium and washing the cells twice with PBS, H_2O_2 at a final concentration of 0.4 mmol·L^{-1} in 2.5% FBS was added. The cells were then incubated for 12 h. Following incubation, the medium was removed, and the level of intracellular ROS in the treated cells was detected (excitation wavelength 488 nm, emission wavelength 525 nm) using fluorescence microscopy (Evident, USA) and spectrophotometry (Therom Scientific, USA). In zebrafish, ROS were stained using DCFH-DA, and the embryo status and changes in ROS levels were observed under a fluorescence microscope (ZEISS, Germany).

2.3.11. Enzyme-linked immunosorbent assay (ELISA) kits for the determination of oxidative stress-related indicators

After treatment, B16F10 cells were harvested and processed according to the protocols provided with the SOD, MDA, CAT, and GSH kits (Elabscience, China). A spectrophotometer (Thermo Scientific, USA) was utilized to measure the absorbance, and subsequently, the levels of SOD, MDA, CAT, and GSH-Px in the B16F10 cells were quantified.

2.3.12. Mitochondrial membrane potential assay

JC-1 serves as a fluorescent probe for assessing mitochondrial membrane potentials. Under normal physiological conditions, JC-1 forms aggregates in the mitochondrial matrix, emitting red fluorescence. However, when the mitochondrial membrane potential decreases, JC-1 fails to aggregate in the matrix and instead exists as a monomer, emitting green fluorescence. The JC-1 monomer has an excitation wavelength of 514 nm and an emission wavelength of 529 nm, while the JC-1 polymer exhibits an excitation wavelength of 585 nm and an emission wavelength of 590 nm [24].

2.3.13. Statistical analysis

All data are presented as the mean ± standard error of the mean (SEM). Each experiment was conducted in triplicate or more. Statistical analysis was performed using one-way ANOVA with Tukey's post hoc test for multiple comparisons. $P < 0.05$ was considered statistically significant. All statistical analyses were conducted using GraphPad Prism 9.4.1 software (GraphPad Software, USA).

3. Results

3.1. HZC promotes melanogenesis

3.1.1. HZC promotes melanogenesis in zebrafish

The change in melanin content in zebrafish serves as a highly visible indicator for assessing the effectiveness of HZC. 1-Phenyl 2-thiourea (PTU), a tyrosinase (Tyr) inhibitor, is widely utilized to suppress pigmentation and enhance optical transparency in zebrafish (*Danio rerio*) embryos [25]. To investigate its impact on melanogenesis, we administered HZC to PTU-treated zebrafish. The findings revealed that melanogenesis was significantly inhibited in the PTU model group, while the melanin content of zebrafish in the PTU water group (where the culture medium was replaced with egg water after PTU modeling) showed partial restoration compared to the model group. Furthermore, in the drug group (where the culture medium was replaced with egg water containing 30 μg·mL^{-1} HZC after PTU modeling), zebrafish exhibited a marked increase in (Fig. 1A).

3.1.2. Effect of HZC on cell viability and melanin biosynthesis

The impact of HZC on cell viability was assessed using the MTT assay. Following 48 h of HZC treatment, no cytotoxicity was observed at concentrations of 1, 10, and 20 μg·mL^{-1} (Fig. 1B). The effects of HZC (at concentrations of 1, 10, and 20 μg·mL^{-1}) on tyrosinase activity in B16F10 cells were evaluated through L-DOPA oxidation (Fig. 1C), while its effects on melanogenesis were determined by NaOH cleavage (Fig. 1D). The findings demonstrated that HZC significantly enhanced both tyrosinase activity and melanin content in B16F10 cells.

3.1.3. HZC promotes the expression of gp100, Mitf and Tyr in B16F10 cells

The glycoprotein 100 (gp100) is associated with the formation of melanosome fibrils and plays a crucial role in melanosome maturation. Microphthalmia-associated transcription factor (Mitf), a key transcriptional regulator, governs melanocyte growth and development. Tyrosinase (Tyr) functions as the critical rate-limiting enzyme in melanin synthesis and is regulated by Mitf [20, 26, 27]. Melanin biosynthesis levels can be indirectly assessed through the measurement of Mitf, gp100, and Tyr. Con-

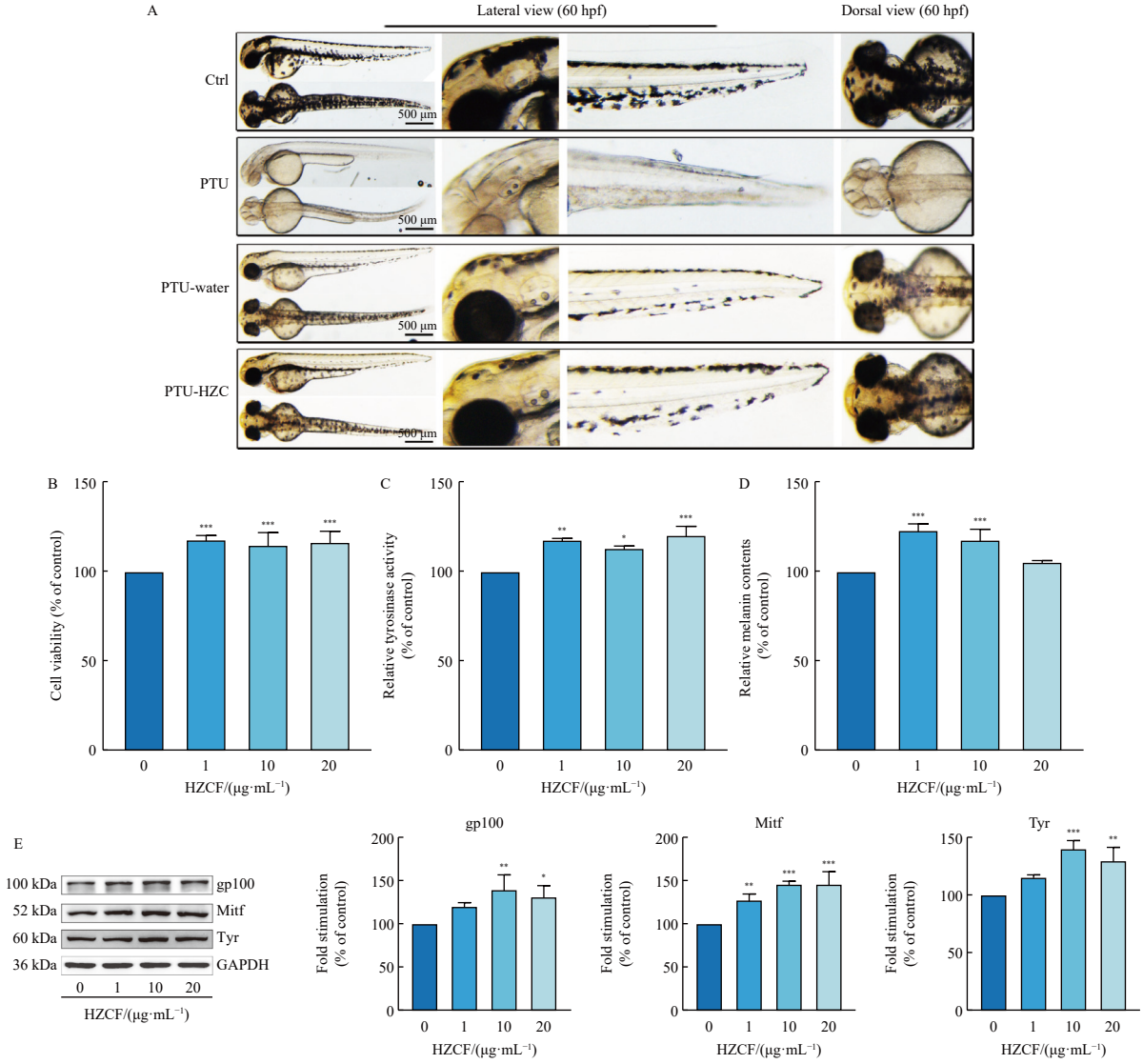

Fig. 1 HZC promotes melanogenesis. (A) HZC promotes melanogenesis in zebrafish, PTU was used as a Control group. (B) B16F10 cells were treated with different concentrations (0,1, 10, 20 μg·mL^{-1}) of HZC. The cell growth inhibition was determined by MTT assay. (C) Effects of different concentrations (0, 1, 10, 20 μg·mL^{-1}) of HZC treatment for 48 h on tyrosinase activity in B16F10 cells. (D) Effects of different concentrations (0, 1, 10, 20 μg·mL^{-1}) of HZC treatment for 48 h on melanin content of B16F10 cells. (E) Treated with HZC (0, 1, 10, 20 μg·mL^{-1}) in B16F10 cells for 48 h, and WB was then applied to detect the protein levels of Tyr, Mitf, gp100. Results are presented as mean ± SEM (n = 3). $^{*}P < 0.05$, $^{**}P < 0.01$, $^{***}P < 0.001$ *vs* control.

sequently, we employed Western blot analysis to evaluate the impact of varying concentrations of HZC (1, 10, 20 μg·mL^{-1}) on the expression of Mitf, gp100, and Tyr, the principal proteins involved in melanogenesis in B16F10 cells. The results indicated that HZC enhanced the protein expression of gp100, Mitf, and Tyr, with the most pronounced effect observed at an HZC concentration of 10 μg·mL^{-1} (Fig. 1E).

3.2. Effect of HZC on melanogenesis proteins in B16F10 cells

3.2.1. Effect of HZC on the MAPK pathway in B16F10 cells

Numerous studies have demonstrated the association between the MAPK pathway and melanogenesis. MAPKs comprise a family of serine/threonine protein kinases [28] activated by external signals or stimuli. Current research on MAPK family signaling primarily focuses on four subfamilies: ERK, *c*-Jun *N*-terminal kinase JNK, p38 mitogen-activated protein kinase (p38 MAPK), and ERK5 [29]. The MAPK pathway is involved in regulating the expression of Mitf, a key transcription factor in melanogenesis. The MAPK pathway plays a crucial role in regulating the expression of Mitf, a key transcription factor in melanogenesis [30]. Consequently, this study investigated the effect of HZC on MAPK pathway proteins. The effects of HZC on three pathways—p38, ERK1/2, and JNK-MAPK—were examined using Western blot assay. The results indicated that the p38, ERK1/2, and JNK-MAPK pathways were activated, with elevated levels of p-p38, p-ERK1/2, and p-JNK observed after 5 min of HZC treatment (Fig. 2A).

3.2.2. Effect of HZC on the PKA pathway in B16F10 cells

The PKA signaling pathway, a cAMP-dependent protein kinase pathway, plays a crucial role in promoting Mitf expression through CREB phosphorylation [31, 32]. Additionally, this pathway is instrumental in regulating melanocyte dendritization and the formation of cross-linked melanocytes [32]. To investigate the impact of HZC on the PKA pathway, we conducted a Western blot analysis. The results revealed that after 30 min of HZC exposure, the PKA pathway was activated, leading to a significant increase in p-CREB levels (Fig. 2B).

3.2.3. Effect of HZC on the Wnt pathway in B16F10 cells

The Wnt pathway plays a crucial role in melanocyte progression and differentiation, with Wnt proteins promoting the development of neural crest cells into pigment cells [33-35]. *β*-Catenin, a key downstream effector of the Wnt pathway, undergoes phosphorylation by CK1 at the Ser45 site. This phosphorylation event triggers subsequent phosphorylation of *β*-catenin by GSK-3β [33, 36, 37]. Mutations at these sites enhance *β*-catenin stability. Active-*β*-catenin (unphosphorylated at Ser45) plays a vital role in stabilizing *β*-catenin adsorption and is functionally active in cell-cell adhesion, mediating its transcriptional activity through the canonical Wnt signaling pathway. When Wnt proteins bind to their receptors, cytoplasmic *β*-catenin stabilization increases, leading to its translocation to the nucleus. There, *β*-catenin interacts with LEF/TCF transcription factors to regulate Mitf transcription [38, 39]. To determine the effects of HZC on Wnt pathway-related proteins at various time points, we conducted a Western blot analysis. The results revealed that the Wnt pathway was activated after 6 h of HZC treatment, with significantly elevated levels of p-GSK-3β, *β*-catenin, and active-*β*-catenin (Fig. 2C).

3.3. Effect of HZC on B16F10 cells under oxidative stress

3.3.1. Effect of HZC on the viability of B16F10 cells under oxidative stress

B16F10 cells in the logarithmic growth phase were seeded

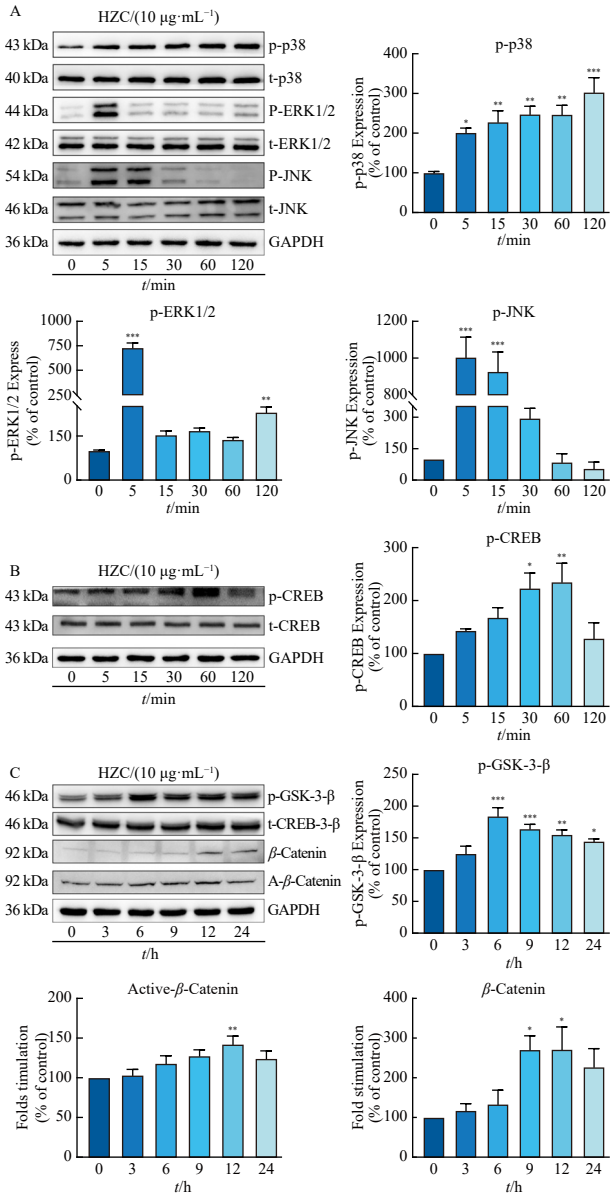

Fig. 2 Effect of HZC on melanogenesis proteins in B16F10 cells. (A) Effects of HZC on the activity of MAPK signaling pathways in melanoma cells B16F10, the p38, ERK1/2, and JNK-MAPK pathways were activated and p-p38, p-ERK1/2, p-JNK protein expression was promoted by WB detection of HZC in B16F10 cells. (B) Effects of HZC on the activity of PKA signaling pathways in melanoma cells B16F10, WB detection of HZC promotion of p-CREB protein expression in B16F10 cells. (C) Effects of HZC on the activity of Wnt signaling pathways in melanoma cells B16F10, WB assay revealed that the Wnt pathway was activated and the levels of p-GSK-3-β, *β*-catenin, and Active-*β*-catenin were significantly elevated. Results are presented as mean ± SEM (n = 3). $^{*}P < 0.05$, $^{**}P < 0.01$, $^{***}P < 0.001$ *vs* control.

into 96-well plates and incubated in DMEM supplemented with 10% FBS in an incubator (37 °C, 5% CO_2) for 24 h. Subsequently, the medium was replaced with DMEM containing 2.5% FBS, and HZC was added to final concentrations of 1, 10, and 20 μg·mL^{-1}. The cells were then incubated for 48 h. Following this, the medium was removed, and the cells were washed twice with PBS. DMEM containing 2.5% FBS and H_2O_2 at a final concentration of 0.4 mmol·L^{-1} was added, and the cells were incubated for an additional 12 h. The impact of HZC on B16F10 cell viability was assessed using the MTT assay. The results indicated that HZC pretreatment did not significantly affect the viability of H_2O_2-treated B16F10 cells (Fig. 3A).

3.3.2. HZC promotes melanin biosynthesis in B16F10 cells under oxidative stress

We investigated the effects of HZC H_2O_2 treatment on tyros-

inase activity and melanogenesis in B16F10 cells using L-DOPA oxidation and NaOH cleavage, respectively. The results demonstrated that H_2O_2 treatment decreased B16F10 tyrosinase activity and melanin content, which was mitigated by HZC pretreatment. Notably, an HZC concentration of 20 μg·mL^{-1} significantly ameliorated the H_2O_2-induced decrease in melanin content. HZC pretreatment dose-dependently increased B16F10 tyrosinase activity and melanin production in H_2O_2-treated B16F10 cells (Fig. 3B). We examined the effects of pretreatment with varying HZC concentrations (1, 10, 20 μg·mL^{-1}) on the expression of key melanogenesis-related proteins, Tyr, Mitf, and gp100, in H_2O_2-treated B16F10 cells *via* the Western blot assay. As illustrated in Fig. 3C, H_2O_2 treatment reduced the expression of these key proteins in B16F10 cells. However, HZC pretreatment dose-dependently attenuated this decrease in protein expression, with the most pronounced effect observed at an HZC concentration of 20 μg·mL^{-1}.

3.3.3. HZC ameliorates the motility of B16F10 cells under oxidative stress

Melanocytes are a crucial component of the epidermis, susceptible to various internal and external factors. Any environmental anomaly in cell growth, proliferation, differentiation, migration, or melanin synthesis can lead to irregularities in melanin formation and deposition, resulting in pigmentation disorders [40]. Vitiligo is characterized by the absence of melanocytes at

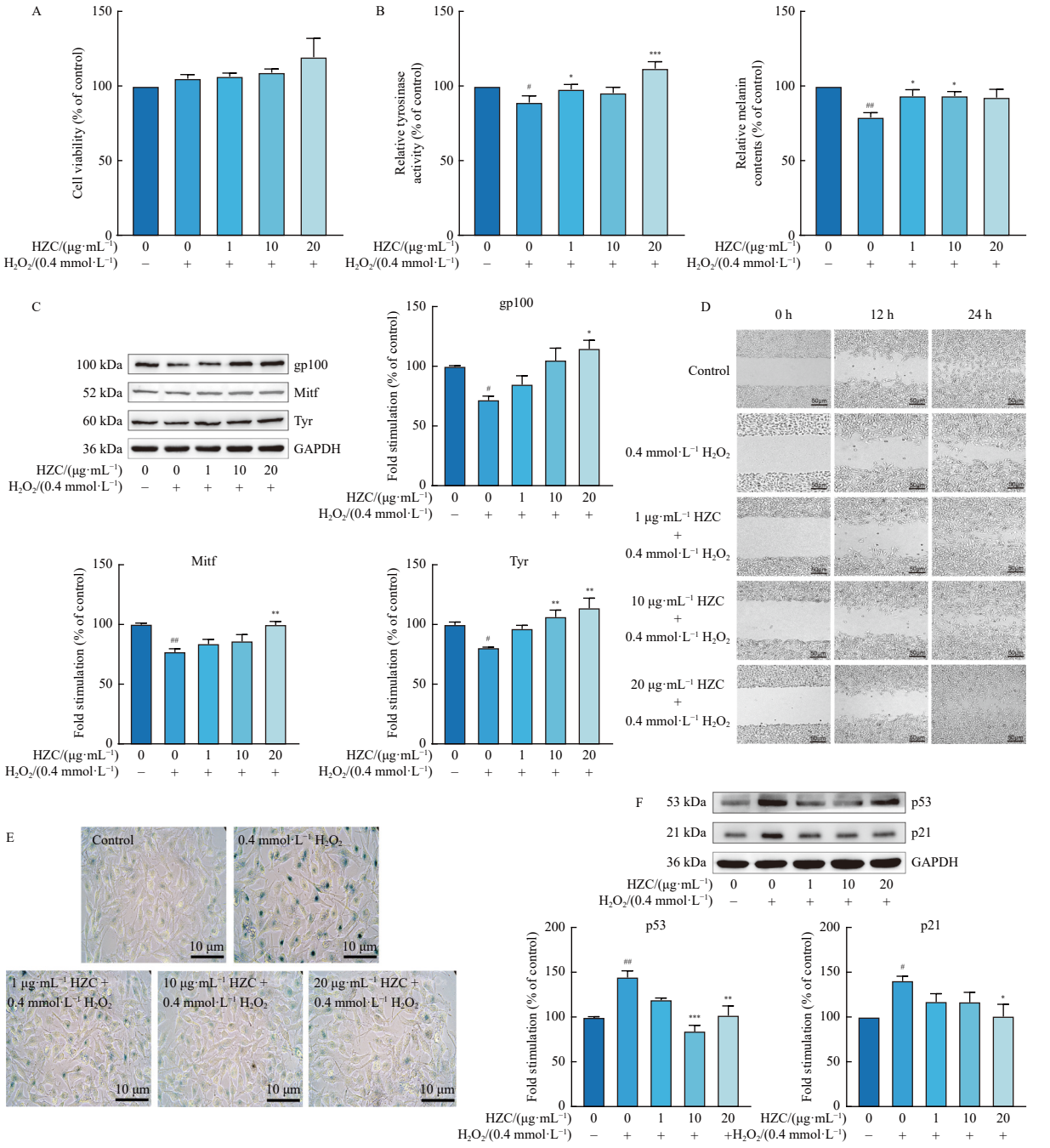

Fig. 3 Effect of HZC on B16F10 cells under oxidative stress. (A) Effect of HZC (0, 1, 10, 20 μg·mL^{-1}) on cell viability in H_2O_2-treated B16F10 for 48 h. (B) Effect of HZC (0, 1, 10, 20 μg·mL^{-1}) on tyrosinase activity and melanin synthesis in H_2O_2-treated B16F10 for 48 h. (C) WB determination of the effect of HZC(0, 1, 10, 20 μg·mL^{-1}) on the protein levels of Mitf, Tyr, and gp100 in H_2O_2-treated B16F10. (D) Effects of HZC on the closure of a pseudo-"wound" field produced by B16F10. (E) Effects of HZC on the *β*-galactosidase activity of H_2O_2-treated B16F10. (F) WB determination of the effect of HZC on the protein levels of p53 and p21 in H_2O_2-treated B16F10. Results are presented as mean ± SEM (n = 3). $^{\#}P < 0.05$, $^{\#\#}P < 0.01$, $^{\#\#\#}P < 0.001$ *vs* control; $^{*}P < 0.05$, $^{**}P < 0.01$, $^{***}P < 0.001$ *vs* model.

the site of the lesion, and it has been found that the recovery of pigmentation at the site of the lesion in patients with advanced vitiligo relies on the production of melanocytes that migrate from nonlesion sites [41, 42]. Following pretreatment with HZC (1, 10, 20 μg·mL^{-1}), H_2O_2-treated B16F10 cells underwent scratch assays, with resulting wounds photographed and observed using an inverted microscope at 0, 12, and 24 h. The scratch assay demonstrated that B16F10 cells gradually migrated into the cell-free area after the appearance of scratches caused by external damage (Fig. 3D). H_2O_2 stimulation decreased the migration ability of B16F10 cells, while HZC pretreatment mitigated this effect and promoted the migration of H_2O_2-treated B16F10 cells into the cell-free area, thereby accelerating scratch repair.

3.3.4. HZC ameliorates oxidative stress-induced premature cell senescence in B16F10 cells

Following pretreatment of B16F10 cells with HZC (1, 10, 20 μg·mL^{-1}) for 48 h, the medium was removed, and cells were washed twice with PBS. DMEM supplemented with 2.5% FBS was added to achieve a final H_2O_2 concentration of 0.4 mmol·L^{-1}, and the mixture was incubated for 12 h. The cells were then stained with *β*-galactosidase (SA-*β*-gal) to analyze the effect of HZC on the premature decrease in H_2O_2-treated cells. H_2O_2 treatment increased the percentage of B16F10 cells with positive staining, significantly differing from the control group. After 48 h of HZC pretreatment, the percentage of positively stained cells was notably lower than in the model group, with the most protective effect observed at 10 μg·mL^{-1} HZC concentration (Fig. 3E). To further investigate HZC's ability to ameliorate senescence in H_2O_2-treated B16F10 cells, we examined the effects of pretreatment with various HZC concentrations (1, 10, 20 μg·mL^{-1}) on the expression of senescence-related proteins p53 and p21 *via* the Western blot assay. The results indicated that H_2O_2 stimulation significantly increased p53 and p21 protein expression (Fig. 3F). However, HZC pretreatment mitigated this effect, with the HZC-treated group showing significantly decreased p53 and p21 expression compared to the model group.

3.4. Effect of HZC on the detachment of B16F10 cells under oxidative stress

3.4.1. HZC ameliorates the attenuation of dendritization in B16F10 cells under oxidative stress

In the cell matrix, actin polymerizes to form microfilaments, which are highly conserved proteins prevalent in eukaryotic cells, and microtubules, which are intermediate fibers that together form the cytoskeleton. Research indicates that microfilaments are associated with various functions, including cell division, adhesion, and motility [43]. Phalloidin, which specifically binds to F-actin, is commonly utilized to detect cytoskeletal morphology [44]. This study employed an actin-tracker green probe for loading, and fluorescence microscopy (Evident, USA) to observe cytoskeletal changes in H_2O_2-treated B16F10 cells after pretreatment with HZC (1, 10, or 20 μg·mL^{-1}). Control group B16F10 cells exhibited normal morphology with an irregular pike shape and pronounced dendritization. H_2O_2 treatment resulted in reduced B16F10 dendritization, with noticeably decreased dendrite length and number (Fig. 4A). HZC mitigated this decrease in dendritization, with dendrite length and number comparable to the control group. The most significant improvement was observed at an HZC concentration of 10 μg·mL^{-1}. Rac1/2/3 and Cdc42, two distinct subfamilies of the Rho protein family [45], play crucial roles in melanocyte dendritization and migratory capacity [46]. Previous research has shown that Rac1/2/3 promotes the formation and elongation of plate-like pseudopods, while Cdc42 encourages the development and extension of filamentous

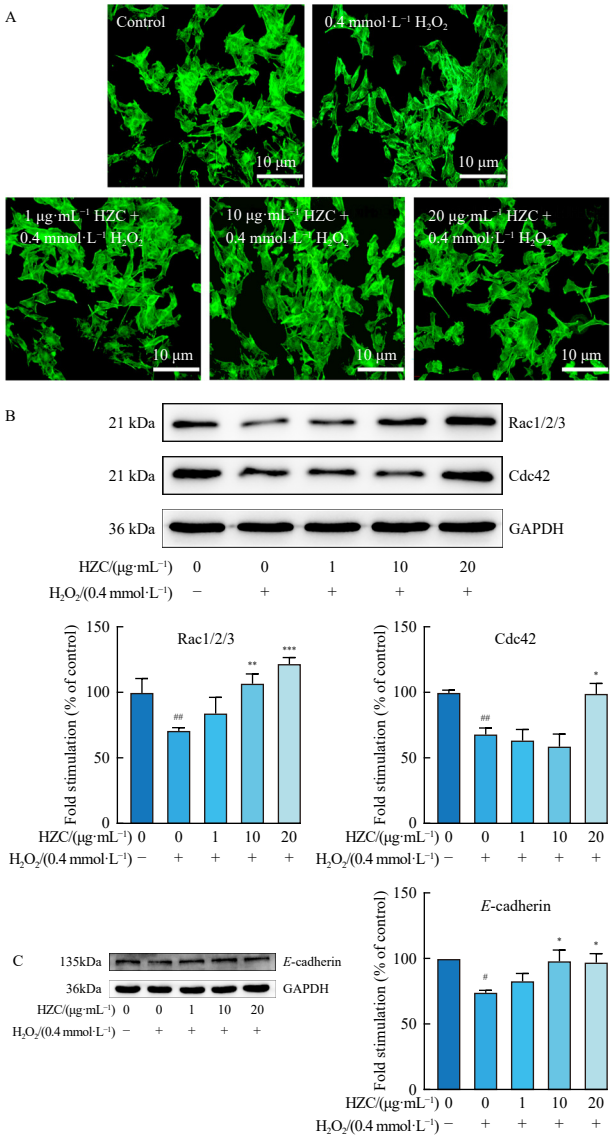

Fig. 4 Effect of HZC on the detachment of B16F10 cells under oxidative stress. (A) Effects of HZC on cytoskeleton of H_2O_2-treated B16F10. (B) Effect of HZC on the protein levels of Rac1/2/3, Cdc42 in H_2O_2-treated B16F10 cells. (C) Effect of HZC on the protein levels of *E*-cadherin in H_2O_2-treated B16F10. Results are presented as mean ± SEM (n = 3). $^{\#}P < 0.05$, $^{\#\#}P < 0.01$, $^{\#\#\#}P < 0.001$ *vs* control; $^{*}P < 0.05$, $^{**}P < 0.01$, $^{***}P < 0.001$ *vs* model.

pseudopods; both proteins inhibit actin depolymerization, stabilize cytoskeletal proteins, and positively regulate dendrite formation [31, 47]. Further investigation of HZC's effect on the cytoskeleton of H_2O_2-treated B16F10 cells *via* the Western blot analysis revealed that H_2O_2 treatment led to downregulation of Rac1/2/3 and Cdc42 protein expression in B16F10 cells. HZC pretreatment dose-dependently ameliorated this decrease in protein expression, with the most pronounced improvement occurring at a concentration of 20 μg·mL^{-1} HZC (Fig. 4B).

3.4.2. HZC ameliorates reduced B16F10 cell adhesion under oxidative stress

E-cadherin serves as a primary mediator of adhesion between melanocytes and keratinocytes in normal human epidermis [48]. Western blot analysis was employed to evaluate the effects of pretreatment with varying concentrations of HZC (1, 10, 20 μg·mL^{-1}) on *E*-cadherin protein expression in H_2O_2-treated B16F10 cells. H_2O_2 treatment resulted in decreased protein expression of *E*-cadherin in B16F10 cells. However, HZC mitigated this reduction in protein expression, with the most significant im-

provement observed at a concentration of 10 μg·mL^{-1} (Fig. 4C).

3.5. HZC ameliorates elevated intracellular ROS levels in B16F10 cells under oxidative stress

Following 48 h treatment of B16F10 cells with 1, 10, 20 μg·mL^{-1} HZC, the medium was replaced with DMEM containing 2.5% FBS and H_2O_2 at a final concentration of 0.4 mmol·L^{-1}, and the cells were incubated for 12 h. HZC pretreatment for 48 h mitigated the H_2O_2-induced elevation in intracellular ROS levels, demonstrating a significant protective effect on B16F10 cells (Fig. 5A). *In vitro* experiments indicated that HZC inhibited ROS production in B16F10 cells under oxidative stress. Subsequently, HZC was applied to zebrafish to examine its effect on ROS generation under oxidative stress. ROS staining in zebrafish using DCFH-DA (10 μmol·L^{-1}) and observation under a fluorescence microscope (Evident, USA) revealed that H_2O_2 treatment significantly increased fluorescence intensity, indicating elevated ROS content compared to the control group. Conversely, HZC pretreatment attenuated the H_2O_2-induced increase in ROS in zebrafish (Fig. 5C).

3.6. HZC ameliorated oxidative damage in B16F10 cells

MAD is a common product of lipid peroxidation *in vivo* and serves as an indirect indicator of the extent of oxidative damage to cells [49]. Under normal physiological conditions, antioxidant enzymes such as SOD, CAT, and GSH-Px eliminate ROS produced by cells, thereby preventing oxidative stress-induced cellular damage [50]. This study utilized a relevant assay kit to measure the levels of these oxidative stress-related biochemical indicators in H_2O_2-treated B16F10 cells exposed to HZC. The results revealed that H_2O_2 treatment led to a significant increase in MAD levels in B16F10 cells, indicating elevated oxidative damage. Additionally, the levels of SOD, CAT, and GSH-Px were altered in the H_2O_2 treatment group compared to the control group. Notably, pretreatment with HZC was able to reverse these effects and mitigate the oxidative damage to the cells (Fig. 6A).

The mitochondrial membrane potential serves as a key indicator of mitochondrial activity, reflecting its functional state. To examine the impact of HZC on mitochondrial function in H_2O_2-stimulated B16F10 cells, we employed JC-1 staining to assess changes in the mitochondrial membrane potential. Following H_2O_2 treatment, a significant reduction in red fluorescence intensity was observed in B16F10 cells, indicative of mitochondrial dysfunction (Fig. 6B). Notably, HZC pretreatment effectively mitigated the H_2O_2-induced decrease in mitochondrial membrane potential. These findings demonstrate that HZC pretreatment exerts a protective effect against mitochondrial dysfunction in H_2O_2-treated B16F10 cells.

3.7. HZC activates the Nrf2-ARE pathway

Nigella sativa L., a widely utilized traditional medicine, has demonstrated antioxidant properties [51]. Previous studies have reported that *Nigella sativa* L. seed extract provides oxidative protection through the Nrf2-ARE pathway in neurodegenerative diseases [52]. To elucidate the potential mechanism of HZC's antioxidant effect in melanocytes, we examined the expression of Nrf2 pathway-related proteins Nrf2, Keap1, HO-1, and NQO1 in B16F10 cells using Western blot analysis. Our findings revealed that HZC increased the expression of antioxidant enzymes HO-1 and NQO1, suggesting an antioxidant role through the activation of the Nrf2-ARE pathway in B16F10 cells (Fig. 7).

4. Discussion

Oxidative stress is a stress response caused by a large accu-

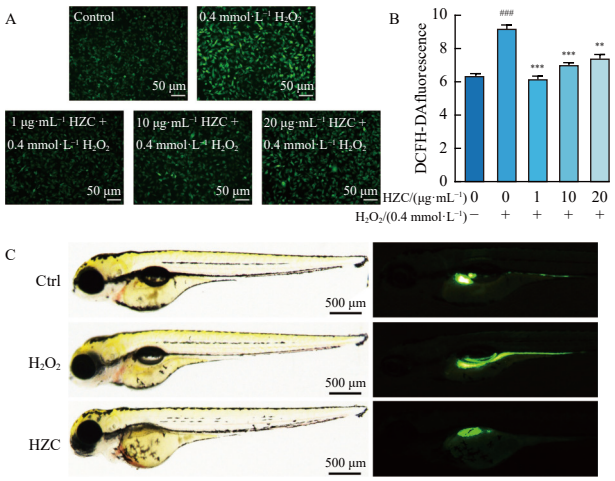

Fig. 5 HZC ameliorates elevated intracellular ROS levels in B16F10 cells under oxidative stress. (A) The protective effect of HZC on H_2O_2-induced ROS generation. (B) Effects of HZC on ROS level of Zebrafish. Zebrafish were treated with egg water containing HZC (30 μg·mL^{-1}) for 24 h, then H_2O_2 (0.5 mmol·L^{-1}) for 4 h. DCFH-DA (10 mmol·L^{-1}) was added to zebrafish for 30 min. Images were captured by fluorescence microscope. Results are presented as mean ± SEM (n = 3). $^{\#}P < 0.05$, $^{\#\#}P < 0.01$, $^{\#\#\#}P < 0.001$ *vs* control; $^{*}P < 0.05$, $^{**}P < 0.01$, $^{***}P < 0.001$ *vs* model.

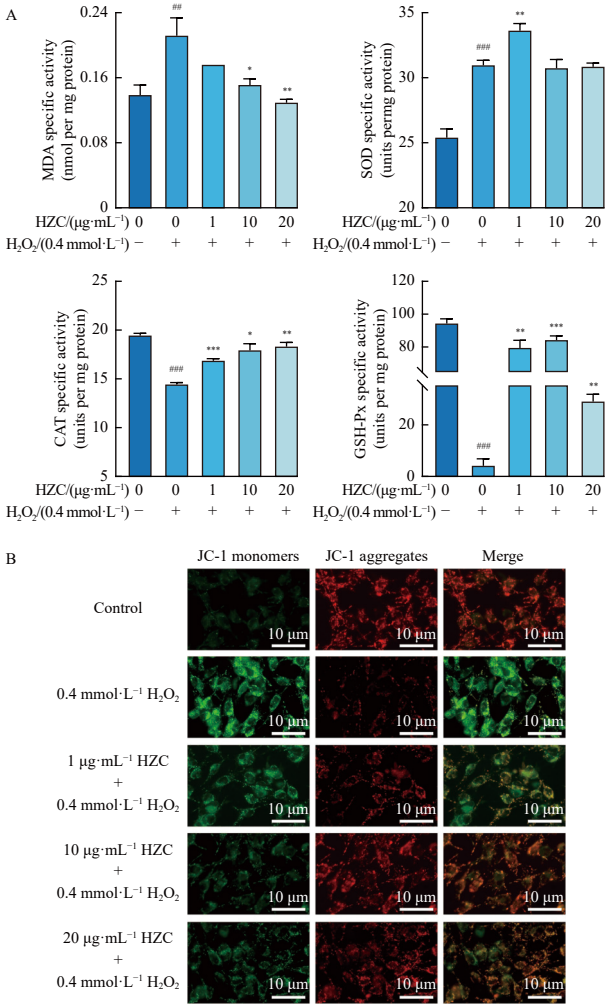

Fig. 6 HZC ameliorated oxidative damage to B16F10 cells. (A) HZC enhances the antioxidant capacity of H_2O_2-treated B16F10 (MDA level, SOD activity, CAT activity, GSH-Px activity). (B) Effect of HZC on the mitochondrial membrane potential in H_2O_2-treated B16F10. Stained with JC-1 fluorescence probe to visualize the mitochondrial membrane potential by fluorescence microscope at 400 × magnification. Results are presented as mean ± SEM (n = 3). $^{\#}P < 0.05$, $^{\#\#}P < 0.01$, $^{\#\#\#}P < 0.001$ *vs* control; $^{*}P < 0.05$, $^{**}P < 0.01$, $^{***}P < 0.001$ *vs* model.

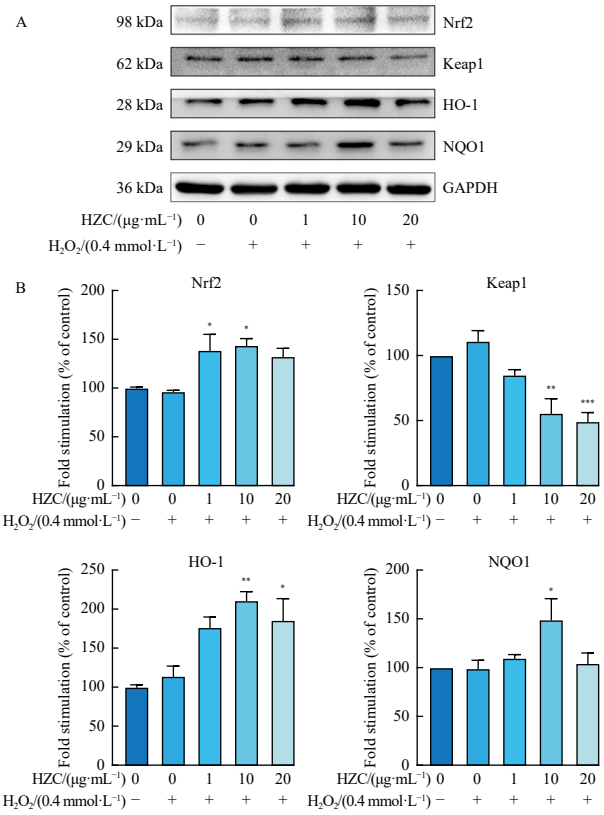

Fig. 7 Effect of HZC on the protein levels of oxidative stress in H_2O_2-treated B16F10. (A) The protein levels of Nrf2, Keap1, HO-1, and NQO1. (B) Quantification of protein expression. Results are presented as mean ± SEM (n = 3). $^{*}P < 0.05$, $^{**}P < 0.01$, $^{***}P < 0.001$ *vs* model.

mulation of ROS in the body, in which the degree of oxidation in the body is greater than the degree of antioxidant oxidative stress; this stress response is a stressful reaction caused by the accumulation of large amounts of ROS in the body [53]. Extensive research has demonstrated that oxidative stress is implicated in the development of various diseases, including inflammation, tumors, neurological disorders, and stress-induced aging [54-57]. Consequently, enhancing the body's antioxidant mechanisms and preventing excessive ROS accumulation are crucial steps in the prevention and treatment of related diseases. The Nrf2-ARE signaling pathway is currently the most extensively studied cellular antioxidant protection mechanism. Nrf2, a nuclear transcription factor, binds to Keap1 under normal physiological conditions, remaining largely inhibited in the cytoplasm. Upon oxidative stimulation, these two proteins dissociate, allowing Nrf2 to be phosphorylated by protein kinases. Nrf2 then translocates to the nucleus, where it recognizes and binds to AREs, initiating the transcription of various downstream antioxidant genes. These downstream antioxidant factors include NQO1, HO-1, CAT, SOD, and GSTs [53, 58-62]. *Nigella sativa* L., a member of the Ranunculaceae family, has a long history of medicinal use among the Uygur people. Its seeds, characterized by a dry, mature taste that is pungent and warm, are traditionally used to treat various ailments, including headaches, eczema, tinnitus, forgetfulness, menstrual irregularities, and lactation issues. Recent studies have demonstrated the significant effect of *Nigella sativa* L. seeds on the repigmentation of skin lesions in vitiligo patients. However, the underlying mechanism remains unexplored. Therefore, we have comprehensively investigated the effects of *Nigella sativa* L. seeds in the treatment of vitiligo, including the mechanism by which they influence melanin formation. Zebrafish embryos, being transparent in their early stages, allow for direct observation of melanin production under an *in vivo* microscope, making them an ideal live animal model for screening melanin production [63]. In this study, we first prepared HZC, an alcoholic extract of *Nigella sativa* L.. We used a zebrafish embryo PTU model to verify the effect of HZC on melanogenesis *in vivo*, and the results demonstrated that HZC promoted melanogenesis in this model (Fig. 1A). To verify the effect of *Nigella sativa* L. extract on melanogenesis *in vitro*, we conducted experiments on the melanoma cell line B16F10. The results showed that HZC increases the viability of B16F10 cells and significantly enhances tyrosinase activity and melanogenesis (Figs. 1B–1D). We further verified that HZC upregulated the expression of the melanogenesis-related proteins gp100, Mitf, and Tyr through Western blot analysis. Moreover, we found that HZC affects melanogenesis by activating the MAPK, PKA, and Wnt-β-catenin pathways (Figs. 1E, 2A–2C).

Vitiligo is a chronic condition characterized by the appearance of white patches on the skin's surface, where oxidative stress stimulation induces premature cellular senescence, leading to melanocyte damage and vitiligo development. This study treated B16F10 cells with 0.4 mmol·L^{-1} H_2O_2 to establish a model of premature melanocyte senescence and detachment, and examined the effect of HZC pretreatment on these cells. Initially, MTT experiments showed no significant increase in cell viability in the HZC pretreated group compared to the control group. Subsequently, we confirmed that HZC has a promelanogenic effect on H_2O_2-treated B16F10 cells. H_2O_2 treatment significantly decreased tyrosinase activity, melanin content, and expression of key melanogenic proteins in B16F10 cells, which was ameliorated by HZC (Figs. 3A–3C). Furthermore, cell scratch repair experiments demonstrated that H_2O_2 treatment reduced B16F10 cell motility, while HZC pretreatment improved this phenomenon, promoting cell migration to the cell-free area and accelerating scratch repair (Fig. 3D) [64]. Activation of p53 leads to periplasmic cell cycle arrest, DNA repair, or apoptosis. In response to certain forms of DNA damage, p53 activates the transcription of its downstream gene, the cyclin-dependent kinase (CDK) inhibitor p21 [65]. To examine cellular senescence, we performed *in situ* β-galactosidase staining of B16F10 cells, revealing that the senescence rate of H_2O_2-treated B16F10 cells was significantly higher than the control, and HZC pretreatment mitigated this alteration (Fig. 3E). Western blot analysis showed that the expression of senescence-related proteins p53 and p21 was significantly elevated in H_2O_2-treated B16F10 cells, while HZC pretreatment decreased the expression of these proteins (Fig. 3F), indicating that HZC alleviates H_2O_2-induced premature senescence in B16F10 cells. Dendritic loss and adhesion defects are the primary causes of melanocyte detachment. We investigated the effect of HZC on the detachment of H_2O_2-treated B16F10 cells. Ghost pen cyclic peptide staining revealed that H_2O_2 treatment decreased dendritic arborization of B16F10 cells, with a significant reduction in dendritic length and number; HZC pretreatment ameliorated this decrease, increasing dendritic length and number (Fig. 4A). Western blot analysis demonstrated that H_2O_2 treatment of B16F10 cells resulted in the downregulation of Rac1/2/3 and Cdc42 protein expression (Fig. 4B), which was dose-dependently ameliorated by HZC pretreatment. Finally, we determined the expression of *E*-cadherin, a key protein involved in melanocyte adhesion, and the results showed that HZC pretreatment ameliorated the H_2O_2-induced decrease in *E*-cadherin expression in B16F10 cells (Fig. 4C).

The skin, functioning as a barrier between the external environment and the human body, is subjected to oxidative stress from both internal and external sources. Excessive ROS generation can adversely affect melanocytes, disrupting their normal metabolism, proliferation, and differentiation, potentially leading to premature cellular senescence and epidermal cell shedding [66]. This study evaluated oxidative stress-related indices in H_2O_2-treated B16F10 cells to explore the potential mechanisms

of HZC intervention in premature melanocyte senescence and detachment. Initially, DCFH-DA staining revealed that HZC significantly reduces H_2O_2-induced ROS increase in B16F10 cells, thereby improving the oxidative damage status of melanocytes (Fig. 5A). Subsequently, zebrafish treated with H_2O_2 and loaded with DCFH-DA probe demonstrated HZC's *in vivo* antioxidant capacity, significantly reducing ROS levels and promoting antioxidant activity (Fig. 5C). Organisms possess various antioxidant molecules, including superoxide dismutase (SOD), CAT, and GSH-Px. SOD converts superoxide anions to O_2 and H_2O_2, while CAT and GSH-Px catalyze the formation of H_2O and O_2; these enzymes collectively scavenge ROS and restore oxidation-reduction equilibrium [53]. Further investigation of HZC's effects on biochemical indices in B16F10 cells revealed that HZC reduced H_2O_2-induced MDA level increase and alleviated cellular oxidative damage, potentially through increased activity of antioxidant enzymes SOD, CAT, and GSH-Px (Fig. 6A). Mitochondria, as cellular energy metabolism centers and primary sites of oxidative phosphorylation, metabolize approximately 90% of cellular oxygen. While aerobic respiration generates ATP, it simultaneously produces substantial O^{2-}, the main ROS source in the body. Under normal physiological conditions, mitochondrial ROS are catalyzed to H_2O and O_2 by antioxidant enzyme systems. Maintaining mitochondrial structural and functional integrity is crucial for basic cellular functions [67]. JC-1 staining demonstrated that HZC pretreatment effectively ameliorated H_2O_2-induced reduction in mitochondrial membrane potential (MMP), thus preserving melanocyte mitochondrial function integrity (Fig. 6B). Under normal physiological conditions, Nrf2 protein levels are low due to Keap1-targeted ubiquitination-dependent proteasomal degradation. Oxidative stress modifies certain Keap1 sensor cysteines, affecting its structure and Nrf2 binding, allowing newly synthesized Nrf2 to accumulate and translocate to the nucleus, activating target genes including *HO-1* and *NQO1* [62, 68, 69]. Western blot analysis revealed that HZC activates the Nrf2-ARE pathway, promoting downstream antioxidant enzyme expression and exerting antioxidant effects (Fig. 7A).

5. Conclusion

In conclusion, HZC demonstrated not only anti-inflammatory, antimicrobial, and antineurological properties but also exhibited potent antioxidative stress effects without cytotoxicity. This antioxidative stress effect can be attributed to HZC's activation of the Nrf2-ARE pathway, which enhances downstream antioxidant enzyme activity, mitigates oxidative damage, and intervenes in melanocyte premature senescence and detachment. Furthermore, the study revealed that HZC promoted melanin production through activation of the MAPK, PKA, and Wnt-β-catenin pathways, improving the condition of H_2O_2-treated melanocytes and restoring melanocyte function. These findings suggest HZC as a potential candidate for vitiligo treatment. However, further research is required to determine whether *Nigella sativa* L. acts through single or multiple components and to address safety considerations.

Funding

This work was supported by the National Natural Science Foundation of China (Nos. 81973410 and 82473537), and the Independent Research Fund of Yunnan Characteristic Plant Extraction Laboratory (Nos. 2022YKZY002 and 2022YKZY004).

Declaration of competing interest

These authors have no conflict of interest to declare.

References

1 Ezzedine K, Eleftheriadou V, Whitton M, et al. Vitiligo. *Lancet*. 2015;386 (9988):74-84. https://doi.org/10.1016/S0140-6736(14)60763-7.
2 Frisoli ML, Harris JE. Vitiligo: mechanistic insights lead to novel treatments. *J Allergy Clin Immunol*. 2017;140(3):654-662. https://doi.org/10.1016/j.jaci.2017.07.011.
3 Sastry KS, Naeem H, Mokrab Y, et al. RNA-seq reveals dysregulation of novel melanocyte genes upon oxidative stress: implications in vitiligo pathogenesis. *Oxid Med Cell Longev*. 2019;2019:2841814. https://doi.org/10.1155/2019/2841814.
4 Hearing VJ. Determination of melanin synthetic pathways. *J Invest Dermatol*. 2011;131(E1):E8-E11. https://doi.org/10.1038/skinbio.2011.4.
5 Zhou S, Zeng H, Huang J, et al. Epigenetic regulation of melanogenesis. *Ageing Res Rev*. 2021;69:101349. https://doi.org/10.1016/j.arr.2021.101349.
6 Boo YC. Human skin lightening efficacy of resveratrol and its analogs: from *in vitro* studies to cosmetic applications. *Antioxidants (Basel)*. 2019;8(9):332. https://doi.org/10.3390/antiox8090332.
7 Lee BW, Schwartz RA, Hercogova J, et al. Vitiligo road map. *Dermatol Ther*. 2012;25(Suppl 1):S44-S56. https://doi.org/10.1111/dth.12006.
8 Picardo M, Dell'Anna ML, Ezzedine K, et al. Vitiligo. *Nat Rev Dis Primers*. 2015;1:15011. https://doi.org/10.1038/nrdp.2015.11.
9 Hara M, Yaar M, Tang A, et al. Role of integrins in melanocyte attachment and dendricity. *J Cell Sci*. 1994;107(Pt 10):2739-2748. https://doi.org/10.1242/jcs.107.10.2739.
10 Gauthier Y, Cario AM, Lepreux S, et al. Melanocyte detachment after skin friction in non lesional skin of patients with generalized vitiligo. *Br J Dermatol*. 2003;148(1):95-101. https://doi.org/10.1046/j.1365-2133.2003.05024.x.
11 Kumar R, Parsad D, Kanwar AJ. Role of apoptosis and melanocytorrhagy: a comparative study of melanocyte adhesion in stable and unstable vitiligo. *Br J Dermatol*. 2011;164(1):187-191. https://doi.org/10.1111/j.1365-2133.2010.10039.x.
12 Menzel N, Schneeberger D, Raabe T. The drosophila p21 activated kinase Mbt regulates the actin cytoskeleton and adherens junctions to control photoreceptor cell morphogenesis. *Mech Dev*. 2007;124(1):78-90. https://doi.org/10.1016/j.mod.2006.09.007.
13 Wagner RY, Luciani F, Cario AM, et al. Altered E-cadherin levels and distribution in melanocytes precede clinical manifestations of vitiligo. *J Invest Dermatol*. 2015;135(7):1810-1819. https://doi.org/10.1038/jid.2015.25.
14 Jian Z, Li K, Song P, et al. Impaired activation of the Nrf2-ARE signaling pathway undermines H_2O_2-induced oxidative stress response: a possible mechanism for melanocyte degeneration in vitiligo. *J Invest Dermatol*. 2014;134(8):2221-2230. https://doi.org/10.1038/jid.2014.152.
15 Hayes JD, McMahon M. NRF2 and KEAP1 mutations: permanent activation of an adaptive response in cancer. *Trends Biochem Sci*. 2009;34(4):176-188. https://doi.org/10.1016/j.tibs.2008.12.008.
16 Lacher SE, Lee JS, Wang X, et al. Beyond antioxidant genes in the ancient Nrf2 regulatory network. *Free Radic Biol Med*. 2015;88(Pt B):452-465. https://doi.org/10.1016/j.freeradbiomed.2015.06.044.
17 Kooti W, Hasanzadeh NZ, Sharafi AN, et al. Phytochemistry, pharmacology, and therapeutic uses of black seed (*Nigella sativa*). *Chin J Nat Med*. 2016;14 (10):732-745. https://doi.org/10.1016/S1875-5364(16)30088-7.
18 Sarac G, Kapicioglu Y, Sener S, et al. Effectiveness of topical *Nigella sativa* for vitiligo treatment. *Dermatol Ther*. 2019;32(4):e12949. https://doi.org/10.1111/dth.12949.
19 Ghorbanibirgani A, Khalili A, Rokhafrooz D. Comparing *Nigella sativa* oil and fish oil in treatment of vitiligo. *Iran Red Crescent Med J*. 2014;16(6):e4515. https://doi.org/10.5812/ircmj.4515.
20 An X, Lv J, Wang F. Pterostilbene inhibits melanogenesis, melanocyte dendricity and melanosome transport through cAMP/PKA/CREB pathway. *Eur J Pharmacol*. 2022;932:175231. https://doi.org/10.1016/j.ejphar.2022.175231.
21 Wang TJ, An J, Chen XH, et al. Assessment of *Cuscuta chinensis* seeds' effect on melanogenesis: comparison of water and ethanol fractions *in vitro* and *in vivo*. *J Ethnopharmacol*. 2014;154(1):240-248. https://doi.org/10.1016/j.jep.2014.04.016.
22 Wang HM, Chen CY, Wen ZH. Identifying melanogenesis inhibitors from *Cinnamomum subavenium* with *in vitro* and *in vivo* screening systems by targeting the human tyrosinase. *Exp Dermatol*. 2011;20(3):242-248. https://doi.org/10.1111/j.1600-0625.2010.01161.x.
23 Westerfield M. *The Zebrafish Book, A Guide for The Laboratory Use of Zebrafish (Danio rerio)*. Inst of Neuro Science, 2000.
24 Tu M, Fan X, Shi J, et al. 2-Fluorofucose attenuates hydrogen peroxide-induced oxidative stress in HepG2 cells *via* Nrf2/keap1 and NF-kappaB signaling pathways. *Life (Basel)*. 2022;12(3):406. https://doi.org/10.3390/life12030406.
25 Chen XK, Kwan JS, Chang RC, et al. 1-Phenyl 2-thiourea (PTU) activates autophagy in zebrafish embryos. *Autophagy*. 2021;17(5):1222-1231. https://doi.org/10.1080/15548627.2020.1755119.
26 Wang R, Chen T, Zhao B, et al. FGF21 regulates melanogenesis in alpaca melanocytes *via* ERK1/2-mediated MITF downregulation. *Biochem Biophys Res Commun*. 2017;490(2):466-471. https://doi.org/10.1016/j.bbrc.2017.06.064.
27 Lee CS, Park M, Han J, et al. Liver X receptor activation inhibits melanogenesis through the acceleration of ERK-mediated MITF degradation. *J Invest Dermatol*. 2013;133(4):1063-1071. https://doi.org/10.1038/jid.2012.409.
28 Kim EK, Choi EJ. Pathological roles of MAPK signaling pathways in human

diseases. *Biochim Biophys Acta*. 2010;1802(4):396-405. https://doi.org/10.1016/j.bbadis.2009.12.009.
29 Lewis TS, Shapiro PS, Ahn NG. Signal transduction through MAP kinase cascades. *Adv Cancer Res*. 1998;74:49-139. https://doi.org/10.1016/s0065-230x(08)60765-4.
30 Kim DS, Park SH, Kwon SB, et al. Sphingosylphosphorylcholine-induced ERK activation inhibits melanin synthesis in human melanocytes. *Pigment Cell Res*. 2006;19(2):146-153. https://doi.org/10.1111/j.1600-0749.2005.00287.x.
31 Busca R, Ballotti R. Cyclic AMP a key messenger in the regulation of skin pigmentation. *Pigment Cell Res*. 2000;13(2):60-69. https://doi.org/10.1034/j.1600-0749.2000.130203.x.
32 Saha B, Singh SK, Sarkar C, et al. Activation of the Mitf promoter by lipid-stimulated activation of p38-stress signalling to CREB. *Pigment Cell Res*. 2006;19(6):595-605. https://doi.org/10.1111/j.1600-0749.2006.00348.x.
33 Amit S, Hatzubai A, Birman Y, et al. Axin-mediated CKI phosphorylation of beta-catenin at Ser 45: a molecular switch for the Wnt pathway. *Genes Dev*. 2002;16(9):1066-1076. https://doi.org/10.1101/gad.230302.
34 Dorsky RI, Moon RT, Raible DW. Control of neural crest cell fate by the Wnt signalling pathway. *Nature*. 1998;396(6709):370-373. https://doi.org/10.1038/24620.
35 Dunn KJ, Brady M, Ochsenbauer JC, et al. WNT1 and WNT3a promote expansion of melanocytes through distinct modes of action. *Pigment Cell Res*. 2005;18(3):167-180. https://doi.org/10.1111/j.1600-0749.2005.00226.x.
36 Liu C, Li Y, Semenov M, et al. Control of beta-catenin phosphorylation/degradation by a dual-kinase mechanism. *Cell*. 2002;108(6):837-847. https://doi.org/10.1016/S0092-8674(02)00685-2.
37 Yanagawa S, Matsuda Y, Lee JS, et al. Casein kinase I phosphorylates the armadillo protein and induces its degradation in Drosophila. *EMBO J*. 2002;21(7):1733-1742. https://doi.org/10.1093/emboj/21.7.1733.
38 Steingrimsson E, Copeland NG, Jenkins NA. Melanocytes and the microphthalmia transcription factor network. *Annu Rev Genet*. 2004;38:365-411. https://doi.org/10.1146/annurev.genet.38.072902.092717.
39 Takeda K, Yasumoto K, Takada R, et al. Induction of melanocyte-specific microphthalmia-associated transcription factor by Wnt-3a. *J Biol Chem*. 2000;275(19):14013-14016. https://doi.org/10.1074/jbc.C000113200.
40 Zhang B, Ma S, Rachmin I, et al. Hyperactivation of sympathetic nerves drives depletion of melanocyte stem cells. *Nature*. 2020;577(7792):676-681. https://doi.org/10.1038/s41586-020-1935-3.
41 Cui J, Shen LY, Wang GC. Role of hair follicles in the repigmentation of vitiligo. *J Invest Dermatol*. 1991;97(3):410-416. https://doi.org/10.1111/1523-1747.ep12480997.
42 Morelli JG, Kincannon J, Yohn JJ, et al. Leukotriene C4 and TGF-alpha are stimulators of human melanocyte migration *in vitro*. *J Invest Dermatol*. 1992;98(3):290-295. https://doi.org/10.1111/1523-1747.ep12497951.
43 Sekino Y, Kojima N, Shirao T. Role of actin cytoskeleton in dendritic spine morphogenesis. *Neurochem Int*. 2007;51(2-4):92-104. https://doi.org/10.1016/j.neuint.2007.04.029.
44 Ning C, Yu P, Zhu Y, et al. Built-in microscale electrostatic fields induced by anatase-rutile-phase transition in selective areas promote osteogenesis. *NPG Asia Mater*. 2016;8:e243. https://doi.org/10.1038/am.2016.9.
45 Wennerberg K, Der CJ. Rho-family GTPases: it's not only Rac and Rho (and I like it). *J Cell Sci*. 2004;117(Pt 8):1301-1312. https://doi.org/10.1242/jcs.01118.
46 Impey S, Davare M, Lesiak A, et al. An activity-induced microRNA controls dendritic spine formation by regulating Rac1-PAK signaling. *Mol Cell Neurosci*. 2010;43(1):146-156. https://doi.org/10.1016/j.mcn.2009.10.005.
47 Scott EK, Reuter JE, Luo L. Small GTPase Cdc42 is required for multiple aspects of dendritic morphogenesis. *J Neurosci*. 2003;23(8):3118-3123. https://doi.org/10.1523/JNEUROSCI.23-08-03118.2003.
48 Tang A, Eller MS, Hara M, et al. E-cadherin is the major mediator of human melanocyte adhesion to keratinocytes *in vitro*. *J Cell Sci*. 1994;107(Pt 4):983-992. https://doi.org/10.1242/jcs.107.4.983.
49 Niki E. Biomarkers of lipid peroxidation in clinical material. *Biochim Biophys Acta*. 2014;1840(2):809-817. https://doi.org/10.1016/j.bbagen.2013.03.020.
50 Zhang J, Wang X, Vikash V, et al. ROS and ROS-mediated cellular signaling. *Oxid Med Cell Longev*. 2016;2016:4350965. https://doi.org/10.1155/2016/4350965.
51 Ardiana M, Pikir BS, Santoso A, et al. Effect of *Nigella sativa* supplementation on oxidative stress and antioxidant parameters: a meta-analysis of randomized controlled trials. *Sci World J*. 2020;2020:2390706. https://doi.org/10.1155/2020/2390706.
52 Dong J, Zhang X, Wang S, et al. Thymoquinone prevents dopaminergic neurodegeneration by attenuating oxidative stress *via* the Nrf2/ARE pathway. *Front Pharmacol*. 2020;11:615598. https://doi.org/10.3389/fphar.2020.615598.
53 Bono S, Feligioni M, Corbo M. Impaired antioxidant KEAP1-NRF2 system in amyotrophic lateral sclerosis: NRF2 activation as a potential therapeutic strategy. *Mol Neurodegener*. 2021;16(1):71. https://doi.org/10.1186/s13024-021-00479-8.
54 Augustin RC, Delgoffe GM, Najjar YG. Characteristics of the tumor microenvironment that influence immune cell functions: hypoxia, oxidative stress, metabolic alterations. *Cancers (Basel)*. 2020;12(12):3802. https://doi.org/10.3390/cancers12123802.
55 Farias JG, Molina VM, Carrasco RA, et al. Antioxidant therapeutic strategies for cardiovascular conditions associated with oxidative stress. *Nutrients*. 2017;9(9):966. https://doi.org/10.3390/nu9090966.
56 Tan BL, Norhaizan ME, Liew WP, et al. Antioxidant and oxidative stress: a mutual interplay in age-related diseases. *Front Pharmacol*. 2018;9:1162. https://doi.org/10.3389/fphar.2018.01162.
57 Hassan W, Noreen H, Rehman S, et al. Association of oxidative stress with neurological disorders. *Curr Neuropharmacol*. 2022;20(6):1046-1072. https://doi.org/10.2174/1570159X19666211111141246.
58 Xiao X, Tong Z, Zhang Y, et al. Novel prenylated indole alkaloids with neuroprotection on SH-SY5Y cells against oxidative stress targeting Keap1-Nrf2. *Mar Drugs*. 2022;20(3):191. https://doi.org/10.3390/md20030191.
59 Lee JM, Johnson JA. An important role of Nrf2-ARE pathway in the cellular defense mechanism. *J Biochem Mol Biol*. 2004;37(2):139-143. https://doi.org/10.5483/bmbrep.2004.37.2.139.
60 Leonard MO, Kieran NE, Howell K, et al. Reoxygenation-specific activation of the antioxidant transcription factor Nrf2 mediates cytoprotective gene expression in ischemia-reperfusion injury. *FASEB J*. 2006;20(14):2624-2626. https://doi.org/10.1096/fj.06-5097fje.
61 Ulasov AV, Rosenkranz AA, Georgiev GP, et al. Nrf2/Keap1/ARE signaling: towards specific regulation. *Life Sci*. 2022;291:120111. https://doi.org/10.1016/j.lfs.2021.120111.
62 Yamamoto M, Kensler TW, Motohashi H. The KEAP1-NRF2 system: a thiol-based sensor-effector apparatus for maintaining redox homeostasis. *Physiol Rev*. 2018;98(3):1169-1203. https://doi.org/10.1152/physrev.00023.2017.
63 Chen YM, Su WC, Li C, et al. Anti-melanogenesis of novel kojic acid derivatives in B16F10 cells and zebrafish. *Int J Biol Macromol*. 2019;123:723-731. https://doi.org/10.1016/j.ijbiomac.2018.11.031.
64 Sikora E, Arendt T, Bennett M, et al. Impact of cellular senescence signature on ageing research. *Ageing Res Rev*. 2011;10(1):146-152. https://doi.org/10.1016/j.arr.2010.10.002.
65 Levine AJ. p53, the cellular gatekeeper for growth and division. *Cell*. 1997;88(3):323-331. https://doi.org/10.1016/S0092-8674(00)81871-1.
66 Bellei B, Picardo M. Premature cell senescence in human skin: dual face in chronic acquired pigmentary disorders. *Ageing Res Rev*. 2020;57:100981. https://doi.org/10.1016/j.arr.2019.100981.
67 Mackenzie RA, Cook MG, Chong H, et al. Senescence evasion in melanoma progression: uncoupling of DNA-damage signaling from p53 activation and p21 expression. *Pigment Cell Melanoma Res*. 2013;26(2):226-235. https://doi.org/10.1111/pcmr.12060.
68 Bellezza I, Giambanco I, Minelli A, et al. Nrf2-Keap1 signaling in oxidative and reductive stress. *Biochim Biophys Acta Mol Cell Res*. 2018;1865(5):721-733. https://doi.org/10.1016/j.bbamcr.2018.02.010.
69 Carpenter EL, Becker AL, Indra AK. NRF2 and key transcriptional targets in melanoma redox manipulation. *Cancers (Basel)*. 2022;14(6):1531. https://doi.org/10.3390/cancers14061531.